

Quantum-enhanced time-of-arrival measuring method based on partially entangled state

Peng-Xian Li(李芃鲜), Lu-Ping Xu(许录平), Gui-Ting Hu(胡桂廷), Wen-Long Gao(高文珑)
Citation: Chin. Phys. B, 2025, 34 (**7**): 070303. DOI: 10.1088/1674-1056/adc7ee
Journal homepage: http://cpb.iphy.ac.cn; http://iopscience.iop.org/cpb

What follows is a list of articles you may be interested in

Probabilistic quantum teleportation of shared quantum secret

Hengji Li(李恒吉), Jian Li(李剑), and Xiubo Chen(陈秀波)
Chin. Phys. B, 2022, 31 (**9**): 090303. DOI: 10.1088/1674-1056/ac67c0

Deterministic hierarchical joint remote state preparation with six-particle partially entangled state

Na Chen(陈娜), Bin Yan(颜斌), Geng Chen(陈赓), Man-Jun Zhang(张曼君), Chang-Xing Pei(裴昌幸)
Chin. Phys. B, 2018, 27 (**9**): 090304. DOI: 10.1088/1674-1056/27/9/090304

Entropy of field interacting with two two-qubit atoms

Tang-Kun Liu(刘堂昆), Yu Tao(陶宇), Chuan-Jia Shan(单传家), Ji-Bing Liu(刘继兵)
Chin. Phys. B, 2018, 27 (**9**): 090303. DOI: 10.1088/1674-1056/27/9/090303

Deterministic joint remote state preparation of arbitrary single- and two-qubit states

Chen Na (陈娜), Quan Dong-Xiao (权东晓), Xu Fu-Fang (徐馥芳), Yang Hong (杨宏), Pei Chang-Xing (裴昌幸)
Chin. Phys. B, 2015, 24 (**10**): 100307. DOI: 10.1088/1674-1056/24/10/100307

Quantum communication for satellite-to-ground networks with partially entangled states

Chen Na (陈娜), Quan Dong-Xiao (权东晓), Pei Chang-Xing (裴昌幸), Yang-Hong (杨宏)
Chin. Phys. B, 2015, 24 (**2**): 020304. DOI: 10.1088/1674-1056/24/2/020304

Quantum-enhanced time-of-arrival measuring method based on partially entangled state

Peng-Xian Li(李芃鲜)[1], Lu-Ping Xu(许录平)[1,†], Gui-Ting Hu(胡桂廷)[1], and Wen-Long Gao(高文珑)[2]

[1] *School of Aerospace Science and Technology, Xidian University, Xi'an* 710126, *China*
[2] *Electronic Engineering Research Institute, Xi'an* 710100, *China*

(Received 14 January 2025; revised manuscript received 24 March 2025; accepted manuscript online 2 April 2025)

We present a quantum ranging protocol that overcomes photon-loss limitations using optimized partially frequency-entangled states. By establishing the fundamental relationship between the degree of entanglement, channel transmission efficiency and measurement precision, we demonstrate superclassical timing resolution in both lossless and lossy regimes. Theoretical analysis and numerical simulations reveal that, under a lossless channel, the precision gain increases with the degree of entanglement, approaching the Heisenberg limit. Importantly, in lossy channels, the precision gain is significantly influenced by both the channel transmission efficiency and the degree of entanglement. For transmission efficiencies above 50%, the proposed method provides up to 1.5 times the precision gain of classical methods when entanglement parameters are optimized. Moreover, by optimizing intra-group and inter-group covariances in the multi-structured entangled state, we achieve substantial precision gains even at low transmission efficiencies ($\sim 30\%$), demonstrating its robustness against loss. This study resolves the critical trade-off between entanglement-enhanced precision and loss-induced information degradation. Future implementation could extend to satellite-based quantum positioning, remote sensing, quantum illumination, and other fields that require high-precision ranging in lossy environments. The protocol establishes a universal framework for loss-tolerant quantum metrology, advancing the practical deployment of quantum-enhanced sensing in real-world applications.

Keywords: quantum ranging, partially entangled state, degree of entanglement

PACS: 03.67.–a, 42.50.–p, 42.50.Dv, 42.50.Ex

DOI: 10.1088/1674-1056/adc7ee **CSTR:** 32038.14.CPB.adc7ee

1. Introduction

The quantum precision ranging method, by utilizing quantum resources, such as quantum entanglement[1] and quantum squeezing,[2] particularly non-classical states of detection, has surpassed the limitations of the standard quantum limit,[3] thereby reaching the measurement precision to the Heisenberg limit.[4,5] Due to its high ranging accuracy, the quantum precision ranging method has found widespread applications, such as in gravitational wave detection,[6,7] quantum imaging,[8–10] biological cell engineering and chemical molecular computation.[11–13] Quantum precision ranging mainly uses the quantum mechanical properties of photons to achieve distance measurement relative to the target objects. Since the ranging problem is essentially a time measurement problem, the quantum precision ranging method also provides ideas for new time synchronization algorithms.[3,14]

In existing schemes, quantum precision ranging schemes based on continuous-variable entangled states enhance measurement precision by utilizing continuous quantum states (such as squeezed states) and quantum entanglement,[15–19] making it highly effective for high-precision short-range measurements in complex environments, achieving near-Heisenberg-limited precision in static environments. However, its sensitivity to environmental decoherence and transmission losses limits its performance, especially in long-distance measurements. In contrast, pulsed quantum ranging methodologies employ pulsed quantum signals (such as quantum radar pulses), which excel in long-range measurements and atmospheric propagation. The brief nature of the pulses and their resistance to signal attenuation makes the pulsed quantum ranging scheme more effective in long-distance and high-noise environments, although it requires precise synchronization and phase control. Overall, the continuous-variable entangled state ranging scheme is suitable for high-precision short-range measurements, while the pulsed quantum ranging scheme offers superior performance in long-distance, atmospheric and fast-target measurements.

In 2001, Giovannetti *et al.* first proposed the theory of pulsed quantum precision ranging.[3] A transmitter sends M pulses to a receiver at various reference points, and distance measurement is achieved by processing the time of arrival (TOA) of the received pulses. According to quantum theory, when the M transmitter pulses are frequency-entangled and number-squeezed containing N quanta, an accuracy gain of $\sqrt{MN}$ times can be obtained theoretically by measuring the correlation in the TOA of the pulses, in comparison to

†Corresponding author. E-mail: Lpxu@mail.xidian.edu.cn

© 2025 Chinese Physical Society and IOP Publishing Ltd. All rights, including for text and data mining, AI training, and similar technologies, are reserved.

the non-entangled case with the same single-photon bandwidth. The accuracy of pulsed quantum ranging in the non-destructive channel is significantly superior to that of classical non-entangled pulse ranging.

In the pulsed quantum ranging scheme, the entangled photons are highly susceptible to photon loss.[3] This implies that once an entangled photon is lost, the entanglement property between the photons is irreversibly compromised. Consequently, the measurement precision of the quantum pulse for a maximally entangled state is significantly diminished.[20] To mitigate the damage caused by photon loss, several ranging schemes have been proposed. In 2007, Shapiro proposed another entangled photon ranging scheme.[21] called 'send-one-detect-all protocol (SODAP)', in which a series of N-photon entangled-state pulses are prepared, with only one photon from each pulse being used to detect the target, while the others are detected within the radar itself. In 2008, Lloyd gave an explanation of how 'quantum illumination' works.[22] Theoretically, quantum illumination based on m-bit entangled photons can achieve a signal-to-noise improvement factor of 2^m compared to non-entangled illumination. Especially in an environment of high loss and strong noise, even if the photon entanglement property is destroyed, quantum illumination can still achieve the improvement of the signal-to-noise ratio.[23,24] It is crucial to emphasize that the principal objective of quantum illumination resides not in distance measurement, but rather in target detection. The application of quantum entanglement properties enables substantial reduction in the minimum error probability during target identification processes, thereby effectively improving the signal-to-noise ratio characteristics.

Here is another strategy to battle the effects of the loss. In 2002, Giovannetti *et al.* discussed using the partially entangled state to replace the maximally entangled state.[20] More complex configurations can be introduced to entangle multiple systems, where different systems have different degrees of entanglement with all other systems. This shows that partial entanglement can protect against loss while still retaining some of the quantum enhancement when the channel transmission efficiency is good.

Previous studies have only suggested that the use of partially entangled states can enhance robustness against loss, without providing an explanation for the underlying reasons. For instance, the accuracy of the average TOA for a partially entangled state with different degrees of entanglement under varying loss conditions has not been discussed. In Section 2, this paper elucidates the principle behind the capacity of partially entangled states to mitigate loss and establishes the relationship between the degree of entanglement and the ability to recover from loss. Moreover, when employing multi-structured entangled systems, all groups involving photon loss are discarded. While this improves loss resilience, it simultaneously wastes the arrival time information of the other photons present in the discarded groups. In Section 3, this paper considers utilizing the TOA of all received photons, rather than those selected after filtering, to estimate the accuracy of the mean TOA and explains the relationship between subsystems and the total system.

2. Analysis of partially frequency-entangled state scheme

The transmitter sends M pulses to the detector, which are frequency-entangled. For simplicity, it is assumed that only one photon is emitted from each mode.

Then, a frequency-entangled state $|\Psi\rangle$ is normalization given by

$$|\Psi\rangle = \int \mathrm{d}\boldsymbol{\omega}\, \psi(\boldsymbol{\omega})\, |\omega_1\rangle_1 |\omega_2\rangle_2 \cdots |\omega_M\rangle_M , \tag{1}$$

where $|\omega_m\rangle_m$ denotes the single-photon, frequency-ω_m state of mode m, and $\psi(\boldsymbol{\omega})$ denotes the spectral function of M photons, in the specific form

$$|\psi(\boldsymbol{\omega})|^2 = \frac{1}{(2\pi)^{\frac{M}{2}} |\boldsymbol{\Sigma}|^{\frac{1}{2}}} \exp\left(-\frac{1}{2}\boldsymbol{\omega}^{\mathrm{T}} \boldsymbol{\Sigma}^{-1} \boldsymbol{\omega}\right). \tag{2}$$

Here, $\boldsymbol{\omega}^{\mathrm{T}} = [\omega_1, \ldots, \omega_M]$, $\boldsymbol{\Sigma}$ is the covariance matrix, $|\Psi\rangle$ is the coherent state if and only if $\boldsymbol{\Sigma}$ is a diagonal matrix, and $|\boldsymbol{\Sigma}\rangle$ is the entangled state if and only if $\boldsymbol{\Sigma}$ is a non-diagonal matrix.

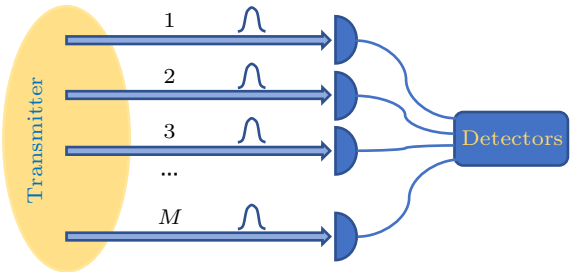


Fig. 1. Schematic diagram of the pulsed quantum ranging scheme.

Assume that $\boldsymbol{\Sigma}$ can be expressed as

$$\boldsymbol{\Sigma} = \begin{bmatrix} \sigma_0^2 & \sigma_1^2 & \cdots & \sigma_1^2 \\ \sigma_1^2 & \sigma_0^2 & \ddots & \vdots \\ \vdots & \ddots & \ddots & \sigma_1^2 \\ \sigma_1^2 & \cdots & \sigma_1^2 & \sigma_0^2 \end{bmatrix}. \tag{3}$$

The elements on the main diagonal are σ_0^2, representing the photon bandwidth of individual modes, while the remaining elements are σ_1^2, indicating the spectral correlation between the two corresponding modes.

When $\sigma_0^2 = \sigma_1^2 \neq 0$, it can be seen that each mode exhibits the maximal entanglement in frequency, implying that the quantum state $|\Psi\rangle$ is the maximally frequency-entangled state. These photons in $|\Psi\rangle$ are indistinguishable, that is, the frequencies are equal. Their frequencies are interrelated through

physical laws such as energy and momentum conservation. The specific relationship depends on the physical process that generates the photons. For instance, in the process of spontaneous parametric down-conversion (SPDC),[25] when a high-frequency photon (such as the signal photon at the frequency ω_{signal}) splits into two lower-frequency photons (such as those photons at the frequency ω_1 and ω_2, respectively), their frequencies are correlated, satisfying relations $\omega_{\text{signal}} = \omega_1 + \omega_2$ and $\omega_1 = \omega_2 = (1/2)\omega_{\text{signal}}$. Similarly, for a four-photon entangled state generated through four-wave mixing,[26] the frequencies (ω_1, ω_2, ω_3 and ω_4) of the four photons satisfy relations $\omega_1 + \omega_2 = \omega_3 + \omega_4$ and $\omega_1 = \omega_2 = \omega_3 = \omega_4$.

Consequently, $\psi(\omega)$ can be simplified as

$$|\psi(\omega)|^2 = \frac{1}{\sqrt{2\pi}\sigma_0^2} \exp\left(-\frac{\omega^2}{2\sigma_0^2}\right). \tag{4}$$

Here, $|\Psi\rangle = \int \mathrm{d}\,\omega\psi(\omega)\,|\omega\rangle\,|\omega\rangle\cdots|\omega\rangle$, and all the modes are in the vacuum state except the one that is at frequency ω. After one photon in the quantum state $|\Psi\rangle$ is measured, it collapses to a particular frequency in that mode with the probability of $|\psi(\omega)|^2$, and the frequencies of the other photons are also determined by the photon's frequency. Therefore, the loss of one photon influences the others, altering the received spectral function $|\psi(\omega)|^2$. In other words, the arrival-time information of other photons encoded in the entanglement cannot be utilized either.

In the absence of photon loss, the accuracy of the average TOA can be expressed as

$$\Delta\tau_{\max} = \frac{1}{2\sigma_0 M}. \tag{5}$$

2.1. Analysis of the time of arrival accuracy for the partially frequency-entangled state under a lossless channel

2.1.1. Methods

When $\sigma_0^2 \neq \sigma_1^2$, it satisfies $\sigma_0^2 > \sigma_1^2 > 0$. It represents a partially entangled state, where, although the degree of frequency entanglement among the photons does not reach its maximum, the measurement of one photon still influences all the others. It is important to note that these photons are distinguishable, meaning their frequencies are not all identical, yet they still adhere to the relevant physical laws. The partially entangled states ranging schemes utilize the information from the non-entangled components that are retained to mitigate the impact of photon loss.

The covariance matrix can be expressed as

$$\boldsymbol{\Sigma} = (\sigma_0^2 - \sigma_1^2)\boldsymbol{I}_M + \sigma_1^2 \boldsymbol{J}_M, \tag{6}$$

which can be decomposed into a unitary matrix $\boldsymbol{I}_M$ and a special matrix $\boldsymbol{J}_M$ of rank 1, $\boldsymbol{J}_M = \mathbf{1}_M \mathbf{1}_M^{\mathrm{T}}$. Thus, the bandwidth of the single photon in individual modes is

$$\sigma_\omega^2 = \sigma_0^2 - \sigma_1^2 + \sigma_1^2 = \sigma_0^2. \tag{7}$$

Since the covariance matrix is symmetric, $\boldsymbol{\Sigma}^{-1}$ exists and is also symmetric, sharing the same form as $\boldsymbol{\Sigma}$. By letting $\boldsymbol{\Sigma}^{-1} = a\boldsymbol{I}_M + b\boldsymbol{J}_M$ and using the method of undetermined coefficient, $\boldsymbol{\Sigma}^{-1}$ can be found as

$$\begin{aligned}\boldsymbol{\Sigma}^{-1} &= \frac{\boldsymbol{I}_M}{\sigma_0^2 - \sigma_1^2} - \frac{\sigma_1^2 \boldsymbol{J}_M}{(\sigma_0^2 - \sigma_1^2 + M\sigma_1^2)(\sigma_0^2 - \sigma_1^2)} \\ &= \frac{1}{(\sigma_0^2 - \sigma_1^2 + M\sigma_1^2)(\sigma_0^2 - \sigma_1^2)} \times \begin{bmatrix} \sigma_0^2 - \sigma_1^2 + (M-1)\sigma_1^2 & -\sigma_1^2 & \cdots & -\sigma_1^2 \\ -\sigma_1^2 & \sigma_0^2 - \sigma_1^2 + (M-1)\sigma_1^2 & \ddots & \vdots \\ \vdots & \ddots & \ddots & -\sigma_1^2 \\ -\sigma_1^2 & \cdots & \sigma_1^2 & \sigma_0^2 - \sigma_1^2 + (M-1)\sigma_1^2 \end{bmatrix},\end{aligned} \tag{8}$$

when no photons are lost, the joint probability density function for receiving M photons is

$$p_{\text{part}} \propto \exp\left[-\frac{\left(\sum_{i=1}^{M} t_i\right)^2}{2 \cdot \frac{1}{4} \cdot \frac{M}{\sigma_0^2 - \sigma_1^2 + M\sigma_1^2}}\right]. \tag{9}$$

The average TOA $\langle t \rangle$ is determined to the following accuracy:

$$\begin{aligned}\Delta\tau_{\text{part}} &= \sqrt{\frac{1}{4} \cdot \frac{M}{\sigma_0^2 - \sigma_1^2 + M\sigma_1^2}} \Big/ M \\ &= \sqrt{\frac{1}{4M(\sigma_0^2 - \sigma_1^2 + M\sigma_1^2)}}.\end{aligned} \tag{10}$$

In comparison to the classical state with the same single-photon bandwidth, where the inverse of the covariance matrix is $\boldsymbol{\Sigma}_{\text{cl}}^{-1} = \boldsymbol{I}_M/\sigma_\omega^2$, the joint probability density function for receiving M non-entangled photons is

$$\begin{aligned}p_{\text{cl}} \propto \prod_{m=1}^{M} \Bigg| \int \mathrm{d}\,\omega_m \frac{1}{(2\pi)^{-1/4}(\sigma_\omega^2)^{-1/4}} \\ \times \exp\left[-\frac{\omega_m^2}{4(\sigma_\omega^2)}\right] \exp(-\mathrm{i}\,\omega_m t_m) \Bigg|^2.\end{aligned} \tag{11}$$

The central limit theorem gives the accuracy of the mean $\langle t \rangle$,

$$\Delta\tau_{\text{cl}} \geq \frac{1}{2\sqrt{M\sigma_0^2}}. \tag{12}$$

The gain in accuracy is expressed as $\Lambda = \Delta\tau_{\rm cl}/\Delta\tau_{\rm part}$. One can derive the following:

$$\Lambda = \sqrt{\frac{\sigma_0^2 - \sigma_1^2 + M\sigma_1^2}{\sigma_0^2}}. \tag{13}$$

That is, in the absence of losses, when $\sigma_1^2 \to \sigma_0^2$, the quantum state $|\Psi\rangle$ tends towards the maximally entangled state, resulting in $\Lambda \to \sqrt{M}$; even for partially entangled states, the accuracy can still exhibit a gain approaching $\sqrt{M}$.

Let $\varepsilon = \sigma_1^2/\sigma_0^2$ be the ratio of covariances, which signifies the degree of entanglement.[27,28] When its value approaches 0, i.e., $\sigma_1^2 \to 0$, this indicates that the entanglement is weaker, approaching a classical state. Conversely, when its value nears 1, i.e., $\sigma_1^2 \to \sigma_0^2$, this suggests a higher degree of entanglement, approaching a maximally frequency-entangled state.

It is now required that the gain in accuracy is greater than 1, which can be expressed as

$$\Lambda = \sqrt{1 - \varepsilon + M\varepsilon} \geq 1. \tag{14}$$

It can be observed that for different values of ε, any arbitrary value of ε can satisfy the requirement.

2.1.2. Results

As depicted in Fig. 2, in the absence of photon loss, for any given value of the degree of entanglement ε, the accuracy of the mean TOA for the partially frequency-entangled state surpasses that of the classical state under identical conditions. The gain Λ exhibits a relatively smooth increase with the degree of entanglement ε and the number of emitted photons M, with the gain approaching $\sqrt{M}$ as $\varepsilon \to 1$.

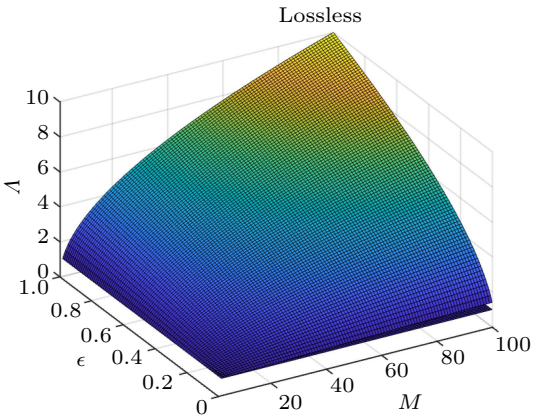


Fig. 2. Gain in accuracy under a lossless channel.

2.2. Analysis of the time-of-arrival accuracy for the partially frequency-entangled state under a lossy channel

2.2.1. Methods

When m photons are received, the received quantum state is formed by selecting the channels that receive photons. The inverse of the covariance matrix is given by

$$\begin{aligned}\boldsymbol{\Sigma}_m^{-1} &= \frac{\boldsymbol{I}_m}{\sigma_0^2 - \sigma_1^2} - \frac{\sigma_1^2 \boldsymbol{J}_m}{(\sigma_0^2 - \sigma_1^2 + M\sigma_1^2)(\sigma_0^2 - \sigma_1^2)} \\ &= \frac{1}{(\sigma_0^2 - \sigma_1^2 + M\sigma_1^2)(\sigma_0^2 - \sigma_1^2)} \times \begin{bmatrix} \sigma_0^2 - \sigma_1^2 + (M-1)\sigma_1^2 & -\sigma_1^2 & \cdots & -\sigma_1^2 \\ -\sigma_1^2 & \sigma_0^2 - \sigma_1^2 + (M-1)\sigma_1^2 & \ddots & \vdots \\ \vdots & \ddots & \ddots & -\sigma_1^2 \\ -\sigma_1^2 & \cdots & \sigma_1^2 & \sigma_0^2 - \sigma_1^2 + (M-1)\sigma_1^2 \end{bmatrix}_{m\times m}. \end{aligned} \tag{15}$$

The joint probability density function for the TOA of m received photons is given by

$$p_{\text{part-}m} \propto \exp\left[-\frac{\left(\sum_{i=1}^{m} t_i\right)^2}{2\Delta\tau_m^2} \right], \tag{16}$$

where

$$\Delta\tau_m = \sqrt{\frac{m}{4} \cdot \frac{\sigma_0^2 - \sigma_1^2 + (M-m)\sigma_1^2}{(\sigma_0^2 - \sigma_1^2 + M\sigma_1^2)(\sigma_0^2 - \sigma_1^2)}}. \tag{17}$$

Therefore, the accuracy of $\langle t \rangle$ is

$$\Delta\tau_{\text{part-}m} = \sqrt{\frac{1}{4m} \cdot \frac{\sigma_0^2 - \sigma_1^2 + (M-m)\sigma_1^2}{(\sigma_0^2 - \sigma_1^2 + M\sigma_1^2)(\sigma_0^2 - \sigma_1^2)}}. \tag{18}$$

Here, it is evident that if a maximally entangled state is used, $\sigma_0^2 = \sigma_1^2$, the measurement precision would be meaningless.

However, the probability $P_{\text{part-}m}$ is not entirely dependent on the situation of a single photon. It is necessary to multiply Eq. (16) by a constant P_m, ensuring that the summation of the probability over all times t_i precisely equals the probability of detecting m photons. The constant P_m is given by

$$P_m \equiv \binom{M}{m} \frac{(\eta)^m (1-\eta)^{M-m}}{1 - (1-\eta)^M}. \tag{19}$$

Here, η represents the received probability of each photon, that is, the channel's transmission efficiency, and $1/(1-(1-\eta)^M)$ is the renormalization factor. Thus, the mean of TOA is obtained by estimating the mean of $\sum_{i=1}^{m} t_i/m$, given by

$$\Delta\bar{\tau}_{\text{part-}m} = \sqrt{\sum_{m=1}^{M} \left(\frac{P_m}{4m} \cdot \frac{\sigma_0^2 - \sigma_1^2 + (M-m)\sigma_1^2}{(\sigma_0^2 - \sigma_1^2 + M\sigma_1^2)(\sigma_0^2 - \sigma_1^2)} \right)}. \tag{20}$$

This is the prior estimation of the arrival-time precision for emitting M photons under a lossy channel.

Compared to the classical state under identical conditions, where M photons are emitted under a lossy channel, the average of TOA is determined to the following accuracy:

$$\Delta\tau_{\text{cl-}m} \geq \frac{1}{2\sqrt{m\sigma_0^2}}. \tag{21}$$

Similarly, after introducing Eq. (19), one can obtain

$$\Delta\bar{\tau}_{\text{cl-}m} = \sqrt{\sum_{m=1}^{M}\left(\frac{P_m}{4m\sigma_0^2}\right)}. \tag{22}$$

Thus, the gain $\Lambda_m = \Delta\bar{\tau}_{\text{cl-}m}/\Delta\bar{\tau}_{\text{part-}m}$ can be derived as

$$\begin{aligned}\Lambda_m &= \sqrt{\frac{\sum_{m=1}^{M}\left(\frac{P_m}{4m\sigma_0^2}\right)}{\sum_{m=1}^{M}\left(\frac{P_m}{4m}\cdot\frac{\sigma_0^2-\sigma_1^2+(M-m)\sigma_1^2}{(\sigma_0^2-\sigma_1^2+M\sigma_1^2)(\sigma_0^2-\sigma_1^2)}\right)}} \\ &= \sqrt{\frac{\frac{\sigma_0^2-\sigma_1^2}{\sigma_0^2}\sum_{m=1}^{M}\frac{P_m}{m}}{\sum_{m=1}^{M}\frac{P_m}{m}-\frac{\sigma_1^2}{\sigma_0^2-\sigma_1^2+M\sigma_1^2}\sum_{m=1}^{M}P_m}}.\end{aligned} \tag{23}$$

Similarly, introducing the degree of entanglement $\varepsilon = \sigma_1^2/\sigma_0^2$, where $0 < \varepsilon < 1$, when the gain Λ_m exceeds 1, the following can be obtained:

$$\Lambda_m = \sqrt{\frac{1-\varepsilon}{1-\kappa_M\frac{\varepsilon}{1-\varepsilon+M\varepsilon}}} \geq 1, \tag{24}$$

where $\kappa_M = \sum_{m=1}^{M}P_m/\sum_{m=1}^{M}\frac{P_m}{m}$ is the introducing parameter related to M and transmission efficiency η. There is no doubt that regardless of how large a value of M is chosen, $1 < \kappa_M < M$ remains constant.

Further calculation of Eq. (24) leads to the range of values for the degree of entanglement when the number of emitted photons M is constant:

$$\varepsilon \in \left[0, \frac{\kappa_M - 1}{M-1}\right]. \tag{25}$$

2.2.2. Results

Focusing on a single simulation subplot in Fig. 3, under a lossy transmission channel, the transmission efficiency η has a significant impact on the gain Λ. The higher the transmission efficiency, the better the gain. In addition, the gain initially increases and then decreases with the degree of entanglement ε. The optimal gain occurs at larger ε for fewer emitted photons and smaller ε for greater photon numbers. This is because the smaller the degree of entanglement, the more pronounced the classical nature of the state becomes. When photon loss occurs, the disruption of the entanglement has less effect on the accuracy of the gain.

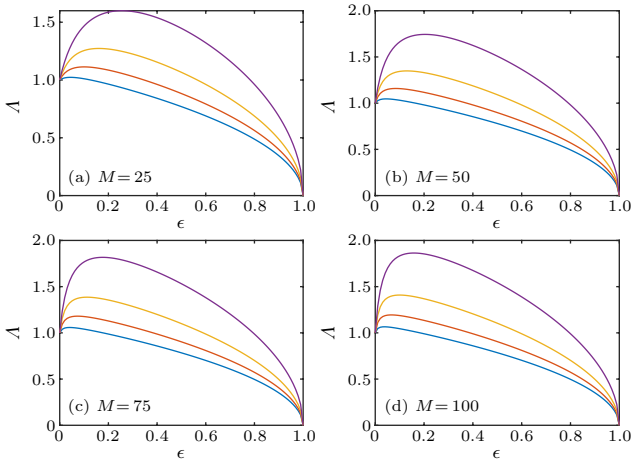


Fig. 3. Relationship between the gain Λ_m and the degree of entanglement ε when the number of emitted photons M is fixed. Blue curve represents $\eta = 20\%$; red curve represents $\eta = 40\%$; yellow curve represents $\eta = 60\%$; purple curve represents $\eta = 80\%$.

Upon comparing the four simulation images in Fig. 3, it can be observed that as the number of emitted photons M increases, the channel transmission efficiency η improves, leading to a greater gain in accuracy. However, the degree of entanglement diminishes when the maximum gain is reached. In accordance with the expression given in Eq. (25), for the partially entangled state to achieve better accuracy than the classical state, the range of values for its degree of entanglement will also be relatively broader.

For a fixed number of emitted photons M propagating through a certain channel with the transmission efficiency η, the constant κ_M remains invariant. The extremum analysis of the function in Eq. (24) yields the value of ε that maximizes the precision gain. However, it is essential to distinguish between different situations rather than making generalized assumptions.

Solving Eq. (24) demonstrates that when $M > \kappa_M + 1$ (which is typically satisfied), the maximum gain is attained at

$$\varepsilon_{\Lambda_{\max}} = \frac{2M - 2 + \sqrt{4\kappa_M M^2 - 4(\kappa_M^2+\kappa_M)M}}{2(M-\kappa_M-1)(1-M)}. \tag{26}$$

When $M < \kappa_M + 1$ (in the rare cases of high transmission efficiency η or few emitted photons M), the gain can reach the maximum at $\varepsilon_{\Lambda_{\max}} = 1$. That is, using the maximally entangled states can achieve the optimum.

When 100 entangled photons are emitted, as the transmission efficiency η increases, the range of choices for the degree of entanglement ε, which aims to achieve measurement precision superior to that of classical partially entangled states, also expands.

Now, for a fixed value of ε, the number of emitted photons also spans a different range of values to guarantee improvement in accuracy. Recalculating Eq. (24) gives

$$M \leq \frac{\varepsilon - 1 + \kappa_M}{\varepsilon}. \tag{27}$$

Hence, the range of values for M is also dependent on κ_M, which together constrain the range of M. It is not the case that an increased number of emitted photons, under the same conditions, automatically leads to greater gains, as demonstrated in Figs. 5 and 6.

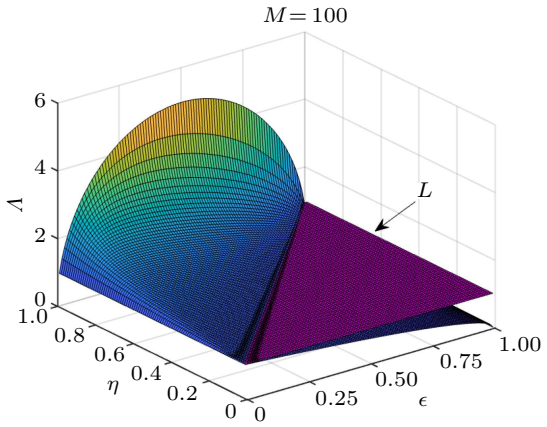


Fig. 4. Gain in accuracy when $M = 100$. Purple plane L in the diagram is the plane of $\Lambda = 1$, with the portion above it indicating that the entangled state provides superior time-of-arrival accuracy, while the portion below it suggests that the classical state offers better time-of-arrival accuracy.

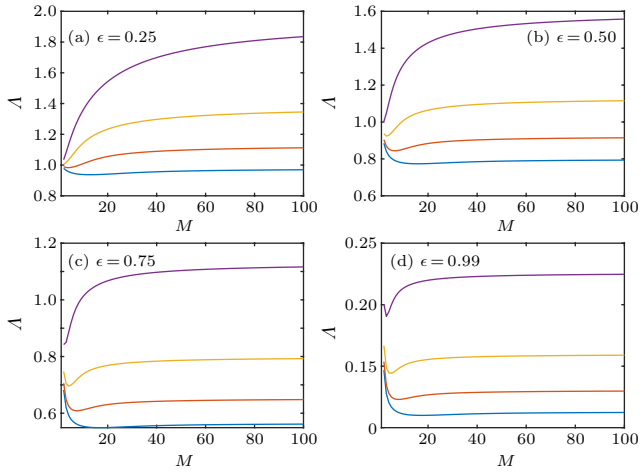


Fig. 5. Relationship between the gain Λ and the number of emitted photons M when the degree of entanglement ε is fixed. Meanings of the colored lines in this figure are consistent with those in Fig. 3.

Precision gain generally improves with increasing emitted photon numbers. However, at high entanglement degrees (e.g., $\varepsilon = 0.99$), the precision gain manifests a pronounced initial decline. The reason for this is that a high degree of entanglement implies that the nature of the entanglement is dominant, and when the number of emitted photons is small, the loss of photons hits the measurement accuracy extremely hard, while it improves when the degree of entanglement is low.

Focusing on the single simulation subplot of Fig. 5, the lower the transmission efficiency of the channel, the greater the number of emitted photons is required to obtain better measurement accuracy using a partially entangled state. Therefore, when the degree of entanglement is fixed — especially at higher levels — attempting to enhance accuracy by increasing the photon transmission has a minimal effect. For example, in the bottom-left subplot titled '$\varepsilon = 0.75$', the transmission efficiency represented by the purple line is $\eta = 80\%$. When $M = 9$, the gain is $\Lambda = 1.0011$; when $M = 16$, it reaches $\Lambda = 1.0530$; when $M = 44$, it just reaches $\Lambda = 1.1000$; when $M = 100$, it only increases to $\Lambda = 1.1162$. It only improved by 0.0162, yet required doubling the number of photons transmitted. The mutual constraints between the transmission efficiency and the number of emitted photons result in a negligible gain in accuracy, in accordance with the reasoning presented in Eq. (27).

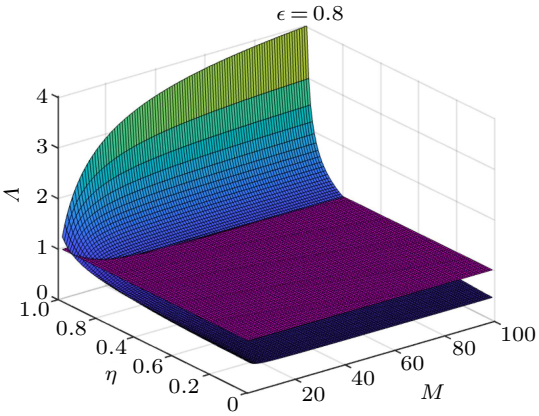


Fig. 6. Gain in accuracy when $\varepsilon = 0.8$. Meaning of the purple plane in this figure is consistent with that in Fig. 4.

When $\varepsilon = 0.8$, a significant improvement in Λ due to an increase in the number of emitted photons only occurs when the channel transmission efficiency is high. When $\eta = 90\%$, if the number of emitted entangled photons exceeds five, using partially entangled states leads to superior accuracy. However, when $\eta = 80\%$, the emitted photons must exceed 100 for the partially entangled state scheme to provide enhanced precision.

It is also important to note that even with a channel transmission efficiency of 90%, the gain when transmitting 100 entangled photons is only 1.4005, which is still significantly lower compared to the nearly ninefold gain in a lossless channel. When the transmission efficiency reaches 98% or 99%, the gains approach 3 and 4, respectively, whereas in a lossless channel, the gain is close to 10. Therefore, when transmitting through a lossy channel, the key consideration in utilizing partially entangled state schemes to enhance precision should be whether to ensure an appropriate degree of entanglement or to ensure a sufficient number of emitted photons.

3. Analysis of multi-structured entangled state schemes

The ranging scheme employing multi-structured entangled states is analogous to that utilizing partially entangled states, as illustrated in Fig. 7.

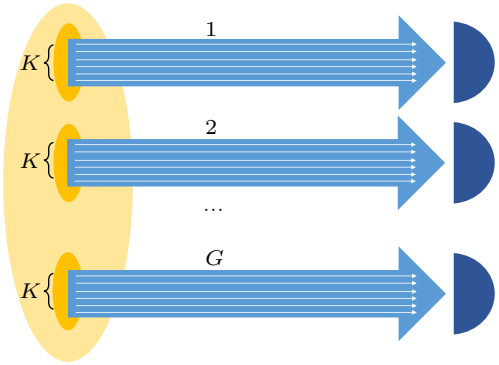


Fig. 7. Schematic diagram of the pulsed quantum ranging scheme using multi-structured entangled states.

Consider the following scenario. A partially entangled state containing M entangled photons is emitted, and these M photons are divided into G groups. The G groups are entangled, while within each group, K photons are also entangled in a manner distinct from the entanglement in the group.

If no photon loss occurs, one can exploit not only the correlations of the K photons within the group but also the correlations between the G groups. In the event of photon loss, however, due to the entanglement structure in place, not all information is inevitably lost.

The emitted quantum state can be represented as follows:

$$|\Psi\rangle_G = \int \mathrm{d}\boldsymbol{\Omega}\Phi(\boldsymbol{\Omega})|\Omega\rangle_1|\Omega\rangle_2\cdots|\Omega\rangle_G, \tag{28}$$

where

$$|\Psi\rangle_j = \int \mathrm{d}\omega\phi(\omega,\Omega)|\omega\rangle_{j1}|\omega\rangle_{j2}\cdots|\omega\rangle_{jK}. \tag{29}$$

This is the state of the jth group of K photons described by one-photon frequency state $|\omega\rangle_{jl}$ for $j = 1,2,\ldots,G$ and $l = 1,2,\ldots,K$.

For the sake of simplicity, let us consider the case of a Gaussian spectrum. That is, $|\Phi(\boldsymbol{\Omega})|^2$ is a Gaussian with a variance of $|\boldsymbol{\Gamma}|$, represented as

$$|\Phi(\boldsymbol{\Omega})|^2 = \frac{1}{(2\pi)^{G/2}|\boldsymbol{\Gamma}|^{1/2}}\exp\left[-\frac{1}{2}\boldsymbol{\Omega}^{\mathrm{T}}\boldsymbol{\Gamma}^{-1}\boldsymbol{\Omega}\right], \tag{30}$$

where $\boldsymbol{\Gamma}$ is the covariance matrix, represented as

$$\boldsymbol{\Gamma} = (\gamma_0^2-\gamma_1^2)\boldsymbol{I}_G+\gamma_1^2\mathbf{1}_G\mathbf{1}_G^{\mathrm{T}} = \begin{bmatrix} \gamma_0^2 & \gamma_1^2 & \cdots & \gamma_1^2 \\ \gamma_1^2 & \gamma_0^2 & \ddots & \vdots \\ \vdots & \ddots & \ddots & \gamma_1^2 \\ \gamma_1^2 & \cdots & \gamma_1^2 & \gamma_0^2 \end{bmatrix}_{G\times G}. \tag{31}$$

Similarly, $|\phi(\omega,\Omega)|^2$ is a Gaussian with a variance of $|\boldsymbol{\Sigma}|$, represented as

$$|\phi(\omega,\Omega)|^2 = \frac{1}{(2\pi)^{K/2}|\boldsymbol{\Sigma}|^{1/2}} \times\exp\left[-\frac{1}{2}(\omega-\Omega)^{\mathrm{T}}\boldsymbol{\Sigma}^{-1}(\omega-\Omega)\right], \tag{32}$$

where $\boldsymbol{\Sigma}$ is the covariance matrix, represented as

$$\boldsymbol{\Sigma} = (\sigma_0^2-\sigma_1^2)\boldsymbol{I}_K+\sigma_1^2\boldsymbol{J}_K = \begin{bmatrix} \sigma_0^2 & \sigma_1^2 & \cdots & \sigma_1^2 \\ \sigma_1^2 & \sigma_0^2 & \ddots & \vdots \\ \vdots & \ddots & \ddots & \sigma_1^2 \\ \sigma_1^2 & \cdots & \sigma_1^2 & \sigma_0^2 \end{bmatrix}_{K\times K}. \tag{33}$$

This multi-structural entangled state can be expressed in two parts. The intra-group part can be viewed as the K-dimensional partially frequency-entangled state, where each channel contains only a single photon. The inter-group part can be considered as the G-dimensional partially frequency-entangled state, where each channel contains K photons.

Similar to the elements in the covariance matrix of partially entangled states, the elements on the main diagonal γ_0^2 and σ_0^2 represent the bandwidth of each group and each photon, respectively, while the off-diagonal elements indicate the correlation between the two corresponding modes.

The generation of multi-structured entangled states is indeed a challenging task. Rather than reconfiguring a multi-photon entangled state into a multi-structured entangled state, an alternative approach might involve recombining multiple entangled states and hybridizing them into a multi-structured entangled state. The following is a straightforward and fundamental idea. A coherent state can be interpreted as an entangled state with the entanglement degree of zero. By hybridizing this coherent state with a maximally entangled state, the resistance to loss can be enhanced. This is the next problem that we will need to solve for verification.

3.1. Analysis of the time-of-arrival accuracy for the multi-structured entangled state under a lossless channel

3.1.1. Methods

In the absence of photon loss, the joint probability density of receiving M photons at the detectors is

$$P_{\text{multistructure-}GK} \propto \exp\left[-\frac{\left(\sum_{j=1}^{G}\sum_{l=1}^{K}t_{j,l}\right)^2}{2\cdot\frac{G}{4(G\gamma^2+\sigma^2)}}\right], \tag{34}$$

where χ^2 and σ^2 correspond to the parameters introduced by $\boldsymbol{\Gamma}^{-1}$ and $\boldsymbol{\Sigma}^{-1}$, respectively, and are expressed as

$$\gamma = \sqrt{\frac{\gamma_0^2-\gamma_1^2+G\gamma_1^2}{G}},\quad \sigma = \sqrt{\frac{\sigma_0^2-\sigma_1^2+K\sigma_1^2}{K}}. \tag{35}$$

Thus, the mean of $\langle t\rangle$ is given by

$$\Delta\tau_{GK} = \sqrt{\frac{G}{4(G\gamma^2+\sigma^2)}}\Big/GK = \frac{1}{2K}\sqrt{\frac{1}{G(G\gamma^2+\sigma^2)}}. \tag{36}$$

A comparison between the multi-structured entangled state and the partially entangled state, exhibits strikingly similar forms. In the calculation, the entanglement in frequency trans-

lates into the bunching of TOA of photons from different pulses. The multi-structured entangled state is divided into two parts for transformation — an inter-group part described by the one-group frequency state $|\Omega\rangle_j$ and an intra-group part described by the one-photon frequency state $|\omega\rangle_{jl}$. This can be viewed as converting the intra-group frequency entanglement of $|\Omega\rangle_j$ into the time domain of the jth group, which is then added to the time domain of the inter-group transformation of $|\Psi\rangle_G$.

Reflected in the time domain, that is, expressed by the inverse of the covariance matrix, it is the sum of the G dimensional diagonal matrix formed by the intra-group σ^2 (Because there is no photon loss, the parameters for each group are equal), and the inverse of the covariance matrix $\boldsymbol{\Gamma}$ for the spectral function of the inter-group part. Thus, the covariance matrix $\boldsymbol{\Gamma}_{\rm s}$ of the ensemble for the multi-structure entangled state can be inversely derived and is expressed as

$$\boldsymbol{\Gamma}_{\rm s} = \sigma^2 \boldsymbol{I}_G + \boldsymbol{\Gamma} = \begin{bmatrix} \gamma_0^2+\sigma^2 & \gamma_1^2 & \cdots & \gamma_1^2 \\ \gamma_1^2 & \gamma_0^2+\sigma^2 & \ddots & \vdots \\ \vdots & \ddots & \ddots & \gamma_1^2 \\ \gamma_1^2 & \cdots & \gamma_1^2 & \gamma_0^2+\sigma^2 \end{bmatrix}_{G\times G}. \quad (37)$$

The bandwidth of each group that contains K photons in $|\Psi\rangle_G$ can be derived as

$$\gamma_{\rm s}^2 = \gamma_0^2 + \sigma^2. \quad (38)$$

Hence, the ratio of covariances of the ensemble can be computed by

$$\varepsilon_{\rm s} = \frac{\gamma_1^2}{\gamma_{\rm s}^2} = \frac{\varepsilon_1}{1+\dfrac{1-\varepsilon_2+K\varepsilon_2}{K\xi_0}}, \quad (39)$$

where $\xi_0 = \gamma_0^2/\sigma_0^2$, representing the ratio of inter-group bandwidth to intra-group bandwidth, is a non-negative value. The entanglement degree of the ensemble $\varepsilon_{\rm s}$ is determined by the actual conditions of the light source, restricting the range of ε_1 for the inter-group covariance matrix $\boldsymbol{\Gamma}$.

From Eq. (39), it can be seen that a multi-structured entangled state is essentially a multi-level nested partially entangled state. The original entanglement degree of the partially entangled state is $\varepsilon_{\rm s}$, and after configuration and nesting, it transforms into a multi-structure entangled state. This results in an increased inter-group entanglement degree ε_1, while the intra-group entanglement degree ε_2 can be arbitrarily adjusted. This adaptability allows the multi-structured entangled state to cope with varying channel transmission efficiencies and mitigate the impact of losses.

Fundamentally, multi-structured entangled states constitute a class of partially entangled states exhibiting intrinsic parameter self-adaptation capabilities.

It can be verified through calculations that, under the lossless channel, the accuracy of $\langle t\rangle$ for the partially entangled state, whose spectral function covariance matrix is $\boldsymbol{\Gamma}_{\rm s}$, is identical to that for the multi-structured entangled state under the same conditions. It can be expressed as

$$\Delta\tau_{\rm s} = \frac{1}{2K}\sqrt{\frac{1}{G(G\gamma^2+\sigma^2)}}. \quad (40)$$

In particular, when the intra-group state is a coherent state with a degree of entanglement of 0, $\varepsilon_2 = \sigma_1^2/\sigma_0^2 = 0$, the bandwidth of a single photon in $|\Psi\rangle_G$ becomes

$$\gamma_{\rm s}^2 = \gamma_0^2 + \sigma_0^2. \quad (41)$$

This represents the bandwidth achieved by employing only the partially entangled state, without utilizing the multi-structured entangled state.

In comparison to the classical state under identical conditions, whose bandwidth of a single photon is $\gamma_{\rm cl}^2 = \gamma_{\rm s}^2 = \gamma_0^2+\sigma_0^2$, the gain in accuracy, $\Lambda_{GK\text{-cl}} = \Delta\tau_{\rm cl}/\Delta\tau_{GK}$, achieved by employing multi-structure entanglement can be derived:

$$\begin{aligned}\Lambda_{GK\text{-cl}} &= \sqrt{\frac{GK\gamma^2}{\gamma_0^2+\sigma_0^2}+\frac{K\sigma^2}{\gamma_0^2+\sigma_0^2}} \\ &= \sqrt{\frac{K}{1+\frac{1}{\xi_0}}\Lambda_{G\text{-}\varepsilon_1}^2+\frac{1}{1+\xi_0}\Lambda_{K\text{-}\varepsilon_2}^2}. \end{aligned} \quad (42)$$

Similar to Eq. (14), both $\Lambda_{G\text{-}\varepsilon_1}$ and $\Lambda_{K\text{-}\varepsilon_2}$ represent the gain for the partially entangled state relative to the classical state. The subscripts G and K denote the number of entangled photons emitted, while ε_1 and ε_2 refer to the corresponding degrees of entanglement. For instance, $\Lambda_{G\text{-}\varepsilon_1}$ represents the precision gain for a partially entangled state, with G entangled photons and the degree of entanglement ε_1.

Upon observing the above Eq. (42), it becomes apparent that the gain can be divided into two components: the gain of the intra-group state to the classical state, and the gain of the inter-group state to the classical state. Optimal gain can be achieved by coordinating parameters such as ξ_0 and K.

3.1.2. Results

Previous investigations[20,29] have numerically demonstrated multi-structured entangled architectures in which maintaining a fixed number of photon groups G, while progressively increasing the photon count per group K, results in an enhanced precision gain through systematic parameter scaling. Simulation results indicate that, under appropriate conditions, emitting more photons using multi-structured entangled states can still effectively improve ranging precision.

Now, let us conduct a simulation, setting the ensemble degree of entanglement to a fixed value, $\varepsilon_{\rm s} = 0.5$, simultaneously balancing the entanglement and classical properties. From Eq. (39), it can be deduced that $\varepsilon_1 > 0.5$ and ε_2 can select arbitrary values within the defined range. Fixing the number of emitted photons, $M = 120$, it is divided evenly into 10, 20, 30 or 40 groups.

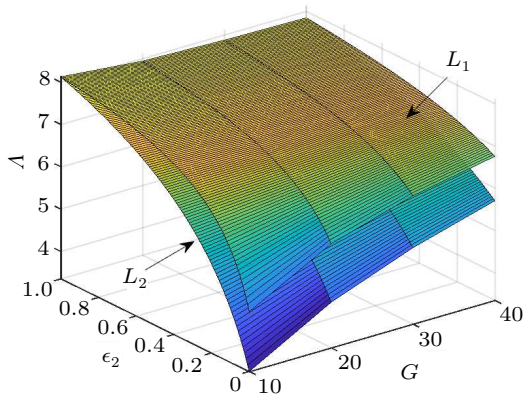


Fig. 8. Multi-structured entangled state versus classical state. Surfaces L_1 and L_2 represent the simulation results for $\varepsilon_1 \approx 0.6$ and $\varepsilon_1 \approx 0.9$, respectively.

We now explore the relationship between $\Lambda_{GK\text{-cl}}$ and both ε_2 and G. Based on the content of Section 2, setting $\varepsilon_1 = 0.6$ or $\varepsilon_1 = 0.9$, the corresponding values of ξ_0 can be determined by different values of ε_2, as derived by Eq. (39). This is illustrated in Fig. 8.

Upon analyzing the results presented in Fig. 8, three distinct features emerge. First, along the ε_2-axis, the gain increases as ε_2 grows, which aligns with the simulation results obtained using the partially entangled state. Second, along the Λ-axis, the surface L_2 lies entirely beneath the surface L_1, meaning that as ε_1 increases, the gain under identical conditions actually decreases, which contrasts with the simulation outcomes for a partially entangled state. Third, along the G-axis, when ε_2 is relatively low, an increase in the number of groups enhances the gain, while at higher values of ε_2, an increase in the number of groups diminishes the gain, resulting in a non-monotonic and non-smooth surface.

It can be derived from Eq. (39) that

$$\xi_0 = \frac{K\varepsilon_2 - \varepsilon_2 + 1}{K\left(\frac{\varepsilon_1}{\varepsilon_s} - 1\right)}, \tag{43}$$

where ε_1, ε_2, ξ_0 and K are interrelated. Along the Λ-axis, ε_2 and K remain constant. Substituting Eq. (43) into Eq. (42) to eliminate ξ_0, it is found that the gain is inversely proportional to ε_1. As ε_1 increases, the gain decreases. Therefore, the surface L_2 lies entirely beneath the surface L_1. We observe that when $\varepsilon_2 = 1$, the gain remains the same regardless of the value of ε_1. This is because $\varepsilon_2 = 1$ signifies that the intra-group states are maximally entangled, and regardless of how many entangled groups are present, there is always the result of $\sigma^2 = \sigma_0^2$. Substituting this into Eq. (43), the ε_s is fixed at 0.5, and as a result, the gain is consistent.

Similarly, along the G-axis, with ε_1 and ε_2 held constant, and applying the elimination method to remove ξ_0 again, the gain in Eq. (42) is a concave function of G. However, it is important to note that the point at which the minimum is reached depends on ε_2. When ε_2 is small, the minimum occurs within the range of $G < 10$, and the gain increases monotonically. As ε_2 increases, the minimum point gradually shifts to the right, with the gain initially decreasing and then increasing. When ε_2 reaches a certain value, the minimum occurs within the range of $G > 40$, and the accuracy gain decreases monotonically. Therefore, the surface is not a smoothly monotonically increasing one.

Under a lossless channel, employing only a partially entangled state, which has the characteristics of $M = 120$, and $\varepsilon = \varepsilon_s = 0.5$ obtains $\Lambda_{M=120,\varepsilon=0.5} = 7.7782$. However, by utilizing a multi-structured entangled state, regardless of the number of groups, we observe that it is possible to achieve a gain, which can be further enhanced by adjusting the ε_2 and G, significantly surpassing the value and resulting in even greater gains. This is more clearly demonstrated in Fig. 10.

As illustrated in Fig. 9, the larger ε_2 becomes, the greater the gain contributed by the intra-group entanglement. With all other conditions being equal, the gain increases, resulting in the surface corresponding to L_1 being the highest, followed by L_2, and L_3 being the lowest. Conversely, as ε_1 increases, the total precision gain diminishes. Therefore, all three surfaces exhibit a downward trend. In summary, as ε_2 increases, the gain becomes less influenced by ε_1, while a smaller ε_2 leads to a greater influence of ε_1 on the gain.

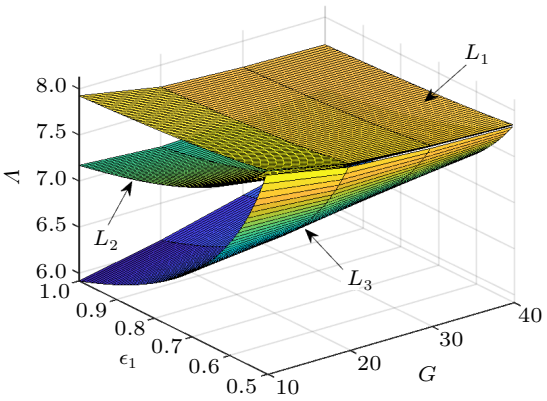


Fig. 9. Multi-structured entangled state versus classical state. Surfaces L_1, L_2 and L_3 represent the simulation results for $\varepsilon_2 \approx 0.3$, $\varepsilon_2 \approx 0.6$, and $\varepsilon_2 \approx 0.9$, respectively.

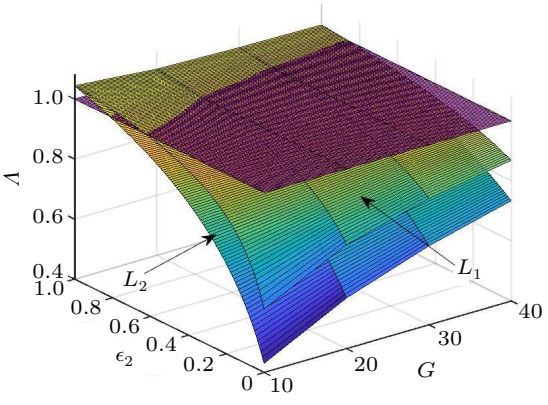


Fig. 10. Multi-structured entangled state versus partially entangled state. Purple plane holds the same meaning as in Fig. 4, while the surfaces L_1 and L_2 have the same meanings as those in Fig. 8.

Consistent with the analysis in Fig. 8, as the number of groups G increases, the gain in Eq. (42) becomes a concave function of G. When $\varepsilon_2 \approx 0.9$, regardless of the value of ε_1, the minimal point is achieved within the range of $G > 40$, resulting in a surface L_1 that is a left-high, right-low slanted curve. When $\varepsilon_2 \approx 0.6$, for smaller values of ε_1, the minimal point is still within the range of $G > 40$, but as ε_1 increases, the minimal point shifts leftwards to the range of $G \in [10, 40]$, and may even be attained when $\varepsilon_1 = 1$, leading to a surface L_2 that is a concave shape with a somewhat gradual change in curvature. When $\varepsilon_2 \approx 0.3$, similarly, for a smaller value of ε_1, the minimal point is within the range of $G > 40$. However, as ε_1 increases, the minimal point shifts leftwards, and upon reaching a certain value, the minimal point is obtained within the range of $G < 10$, thus creating a surface L_3 characterized by a more pronounced, sharply changing distorted shape.

By adjusting ε_1, ε_2 and G, the parameters K and ξ_0 are effectively tuned. These two parameters are interdependent, which results in the gain sometimes decreasing, and the simulation surface exhibiting a concave shape. However, the extremes of this concave point are not significantly different. Therefore, it can be broadly concluded that by using a lower value of ε_1, a higher value of ε_2 to obtain a higher ξ_0, and maximizing the number of photons of K contained in each group, one can attain an optimal gain for the multi-structured entangled state.

In comparison, for a partially entangled state under the same conditions as the emission source — namely, emitting M entangled photons with the bandwidth of a single photon identical to that of the multi-structured entangled state, and with the degree of entanglement ε_S of the ensemble, its form is the same as Eq. (1) — the gain is expressed as $\Lambda_{GK\text{-part}} = \Delta\tau_{\text{part}}/\Delta\tau_{GK}$. After substitution, it can be represented as

$$\begin{aligned}\Lambda_{GK\text{-part}} &= \Delta\tau_{\text{part}}/\Delta\tau_{GK} = \frac{\Lambda_{GK\text{-cl}}}{\Lambda_{\text{part-cl}}} \\ &= \sqrt{\frac{K}{1+\frac{1}{\xi_0}}\frac{\Lambda^2_{G_\varepsilon_1}}{\Lambda^2_{M_\varepsilon_S}} + \frac{1}{1+\xi_0}\frac{\Lambda^2_{K_\varepsilon_2}}{\Lambda^2_{M_\varepsilon_S}}}. \end{aligned} \tag{44}$$

In fact, this is equivalent to scaling the result of Eq. (42) by a factor of $\Lambda_{M=120_\varepsilon=0.5} = 7.7782$. The simulation results are shown in Figs. 10 and 11. The surfaces above the plane L represent the precision enhancement achieved under the same light source conditions by adjusting K and ξ_0.

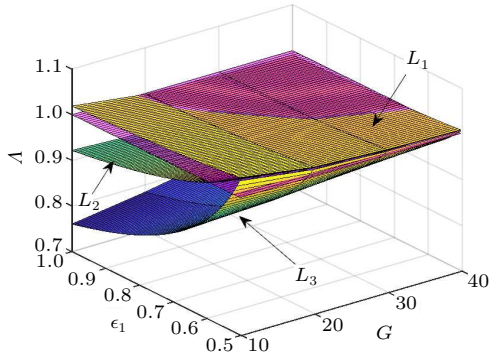


Fig. 11. Multi-structured entangled state versus partially entangled state. Purple plane holds the same meaning as in Fig. 4, while the surfaces L_1, L_2 and L_3 have the same meanings as those in Fig. 9.

Overall, as ε_1 decreases, ε_2 increases and K becomes larger, it becomes easier to achieve a greater gain than that obtained using the partially entangled state. With the degree of entanglement of the emitted light source fixed, one can transition to the multi-structure entangled state to enhance the precision gain in this manner.

3.2. Analysis of the time-of-arrival accuracy for the multi-structured entangled state under a lossy channel

3.2.1. Methods

The previous studies by Giovannetti *et al.*[20] also considered the scenario of employing a multi-structured entangled state in the presence of photon loss. The article examines the situation where, under identical conditions, any group experiencing photon loss is immediately discarded, and only the groups with no photon loss are used to construct the received quantum state. However, the probability of photon loss is the same for each photon, and a sufficient number of groups without photon loss can only be obtained when the channel transmission efficiency is high. Likewise, it also leads to the waste of measurements of the other photons in the groups where photon loss occurs.

This paper considers the computation based on the measurement data of all the received photons, regardless of whether other photons in the group are missing. Under a lossy channel, the received quantum state can be represented as follows. Suppose there are g groups of received photons, and in the jth group, k_j photons are received for $j = 1, 2, \ldots, g$. Then, m photons are received, where $m = \sum_{j=1}^{g} k_j$. The inverse of the covariance matrix $\boldsymbol{\Sigma}$ in Eq. (33), similar to that in Eq. (15), becomes

$$\begin{aligned}\boldsymbol{\Sigma}^{-1}_{k_j} &= \frac{\boldsymbol{I}_{k_j}}{\sigma_0^2-\sigma_1^2} - \frac{\sigma_1^2 \boldsymbol{J}_{k_j}}{(\sigma_0^2-\sigma_1^2+K\sigma_1^2)(\sigma_0^2-\sigma_1^2)} \\ &= \frac{1}{(\sigma_0^2-\sigma_1^2+K\sigma_1^2)(\sigma_0^2-\sigma_1^2)} \times \begin{bmatrix} \sigma_0^2-\sigma_1^2+(K-1)\sigma_1^2 & -\sigma_1^2 & \cdots & -\sigma_1^2 \\ -\sigma_1^2 & \sigma_0^2-\sigma_1^2+(K-1)\sigma_1^2 & \ddots & \vdots \\ \vdots & \ddots & \ddots & -\sigma_1^2 \\ -\sigma_1^2 & \cdots & -\sigma_1^2 & \sigma_0^2-\sigma_1^2+(K-1)\sigma_1^2 \end{bmatrix}_{k_j \times k_j}. \end{aligned} \tag{45}$$

The corresponding parameters σ_j^2 for the jth group are introduced as

$$\sigma_j^2 = \frac{(\sigma_0^2 - \sigma_1^2 + K\sigma_1^2)(\sigma_0^2 - \sigma_1^2)}{k_j\left[\sigma_0^2 - \sigma_1^2 + (K-k_j)\sigma_1^2\right]}. \tag{46}$$

Furthermore, for the inter-group part, it can be considered as a collective of g groups, containing a partially frequency-entangled state with k_j photons in the jth group. The joint probability density of receiving m photons at the detectors is

$$P_{gk} \propto \exp\left[-\frac{\left(\sum_{j=1}^{g}\sum_{l=1}^{k_j} t_{j,l}\right)^2}{2\cdot\frac{1}{4\gamma_g^2}} - \sum_{j=1}^{g}\frac{\left(\sum_{l=1}^{k_j} t_{j,l}\right)^2}{2\cdot\frac{1}{4\sigma_j^2}}\right], \tag{47}$$

where

$$\gamma_g^2 = \frac{\left(\gamma_0^2 - \gamma_1^2 + G\gamma_1^2\right)\left(\gamma_0^2 - \gamma_1^2\right)}{g\left[\gamma_0^2 - \gamma_1^2 + (G-g)\gamma_1^2\right]}.$$

The right-side part represents the intra-group entanglement in frequency translating into the bunching of TOA of photons from different groups, which exhibit coherent properties. Therefore, according to the Lindeberg–Feller central limit theorem, the accuracy is

$$\Delta\tau_{gk} \geq \sqrt{\frac{\sum_{j=1}^{g}\frac{1}{\sigma_j^2}}{1+\gamma_g^2\sum_{j=1}^{g}\frac{1}{\sigma_j^2}}} \Big/ 2\sum_{j=1}^{g} k_j. \tag{48}$$

From the above Eq. (48), it can be discerned that in the presence of photon loss, the arrival-time accuracy is not only dependent on the number of received groups g and the number of photons k_j in the jth group, but also influenced by γ^2 and σ^2 with the variation of the covariance matrix $\boldsymbol{\Gamma}_g$ for the g groups and $\boldsymbol{\Sigma}_j$ for the jth group, respectively.

Similarly, this probability P_{GK_loss} is not entirely dependent on the case of a single photon and a single group. In the jth group, it is necessary to multiply by the same constant $P_{k_j} \equiv \binom{K}{k_j}\frac{(\eta)^{k_j}(1-\eta)^{K-k_j}}{1-(1-\eta)^K}$, as in Eq. (19), while among groups, a different constant P_g' must be multiplied. This ensures that the summation of the probability P_{GK_loss} over all time t_{jl} precisely corresponds to the probability of detecting m photons. In fact, receiving g groups represent the situation where photons from each of these g groups have not been completely lost. In other words, the constant P_g' is complementary to the probability that exactly G–g groups of photons have been entirely lost. Therefore, the constant P_g' can be written as

$$P_g' \equiv 1 - \binom{G}{G-g}\frac{\left[(1-\eta)^K\right]^{G-g}\left[1-(1-\eta)^K\right]^g}{1-\left[(1-\eta)^K\right]^G}, \tag{49}$$

where η represents the transmission efficiency for every channel, and the factor $1-\left[(1-\eta)^K\right]^G$ is introduced for normalization purposes.

The arrival-time accuracy under a lossy channel is given by

$$\Delta\bar{\tau}_{gk} = \sqrt{\sum_{g=1}^{G}\frac{P_g'\sum_{j=1}^{g}\sum_{k_j=1}^{K}\frac{P_{k_j}}{\sigma_j^2}}{4\left(\sum_{j=1}^{g}\sum_{k_j=1}^{K}k_j\right)^2\left(1+\gamma_g^2\sum_{j=1}^{g}\sum_{k_j=1}^{K}\frac{P_{k_j}}{\sigma_j^2}\right)}}. \tag{50}$$

Similarly, compared with the classical state, under identical emission conditions and channel transmission efficiency, the gain of $\Lambda_{gk\text{-cl}} = \Delta\bar{\tau}_{\text{cl}}/\Delta\bar{\tau}_{gk}$ can be expressed as

$$\begin{aligned}\Lambda_{gk\text{-cl}} &= \frac{\Delta\bar{\tau}_{\text{cl}}}{\Delta\bar{\tau}_{gk}} \\ &= \sqrt{\frac{\sum_{m=1}^{M}\frac{P_m}{4m(\gamma_0^2+\sigma_0^2)}}{\sum_{g=1}^{G}\frac{P_g'\sum_{j=1}^{g}\sum_{k_j=1}^{K}\frac{P_{k_j}}{\sigma_j^2}}{4\left(\sum_{j=1}^{g}\sum_{k_j=1}^{K}k_j\right)^2\left(1+\gamma_g^2\sum_{j=1}^{g}\sum_{k_j=1}^{K}\frac{P_{k_j}}{\sigma_j^2}\right)}}}.\end{aligned} \tag{51}$$

In comparison, for a partially entangled state under the same conditions as the emission source, the gain is expressed as $\Lambda_{gk\text{-part}} = \Delta\tau_{\text{part}}/\Delta\tau_{gk}$. After substitution, it can be represented as

$$\Lambda_{gk\text{-part}} = \frac{\Delta\bar{\tau}_m}{\Delta\bar{\tau}_{gk}} = \frac{\Lambda_{gk\text{-cl}}}{\Lambda_{\text{part-cl}}}. \tag{52}$$

3.2.2. Results

In the case of using a multi-structured entangled state, previous studies primarily simulate the relationship between precision gain $\Lambda_{gk\text{-cl}}$ and both the number of groups G and the transmission efficiency η, with the fixed number of photons for each group K and the ratio of inter-group bandwidth to intra-group bandwidth, ξ_0. Their findings indicate that, under conditions of favorable channel transmission efficiency ($\eta \geq 70\%$), employing the multi-structured entangled state can effectively counter photon loss. Their simulation results generally align with our previous inference in Subsection 3.1.2 that the larger the ξ_0 and the higher the K, the greater the precision gain that can be achieved.

In their study, they assume that both intra-group and inter-group states are maximally entangled, while the quantum state of the ensemble remains partially entangled. This requires discarding the entire group in the event of photon loss within a group. In contrast, this paper assumes that both intra-group and inter-group states are partially entangled, thereby enabling the utilization of the TOA information from all received photons.

When we conduct the simulations under identical conditions to those in Subsection 3.1.2, $\varepsilon_{\text{s}} = 0.5$, $M = 120$, and the photons are evenly divided into 10, 20, 30 and 40 groups, respectively.

When ε_1 is fixed at different values, these simulations investigate the relationship between $\Lambda_{gk\text{-cl}}$ and both ε_2 and G for Eq. (51).

We focus on the individual panel in Fig. 12. Under a lossy channel, as the channel transmission efficiency η increases, the gain in accuracy $\Lambda_{gk\text{-cl}}$ decreases. This is because the value of $\Lambda_{gk\text{-cl}}$ is a relative value, rather than an absolute one. When the channel transmission efficiency is low, the measurement precision for the classical state suffers severe degradation, despite being superior to the partially entangled state, whereas that for the multi-structured entangled state performs significantly better by comparison. As one would logically expect, the accuracy of the average TOA obtained by the multi-structured entangled state is a smaller value at a lower transmission efficiency than at a higher transmission efficiency.

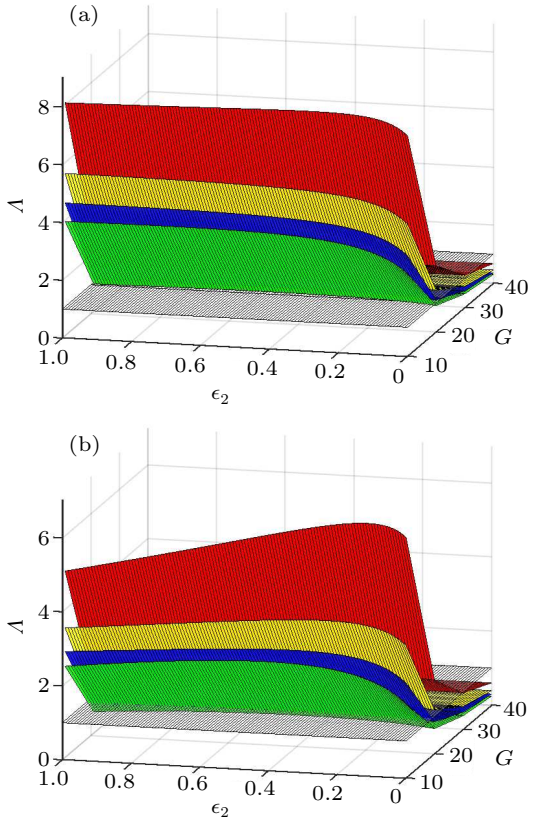


Fig. 12. Multi-structured entangled state versus classical state. Panel (a) represents the simulation results for $\varepsilon_1 \approx 0.6$; panel (b) represents the simulation results for $\varepsilon_1 \approx 0.8$. Red, yellow, blue, and green surfaces represent the simulation results for channel transmission efficiencies of 0.2, 0.4, 0.6 and 0.8, respectively. Gray plane indicates the plane where the gain is equal to 1.

By employing a multi-structured entangled state, as the number of groups G increases, the number of photons of each group K decreases, significantly increasing the probability of losing all photons within the entire group. Although increasing the number of groups G enhances the gain, the higher likelihood of losing all photons in a group proves far more detrimental, diminishing the gain to a greater extent. Conversely, when the number of photon groups G decreases and the number of photons per group K increases, the probability of losing the photons of the entire group is minimal since there is the probability of all K photons being successfully received. As long as the photons are not completely lost in this group, it contributes positively to the gain for the entanglement among groups. This is the reason there is still a significant gain when the number of groups G is small, as well as why the use of a multi-structured entangled state provides superior resistance to loss.

We compare Figs. 12(a) and 12(b). Except the gain increases with ε_2 reflected in the green, blue, and yellow surfaces for the case of $G = 10$ and $\varepsilon_1 \approx 0.6$, in other instances, the values first increase and then decrease as ε_2 increases. This behavior is largely consistent with the simulation results in Fig. 3. The anomalous behavior can be explained as follows. When ε_1 and G are small, ξ_0 is correspondingly large, positively contributing to the ensemble gain. Meanwhile, the reduction in channel transmission efficiency negatively impacts the gain. Thus, when the transmission efficiency is relatively high, the negative influence on the gain is not as pronounced as the negative influence on the gain due to ξ_0, resulting in a total increasing trend.

When ε_1 is fixed at different values, the simulations investigate the relationship between $\Lambda_{gk\text{-part}}$ and both ε_2 and G for Eq. (52).

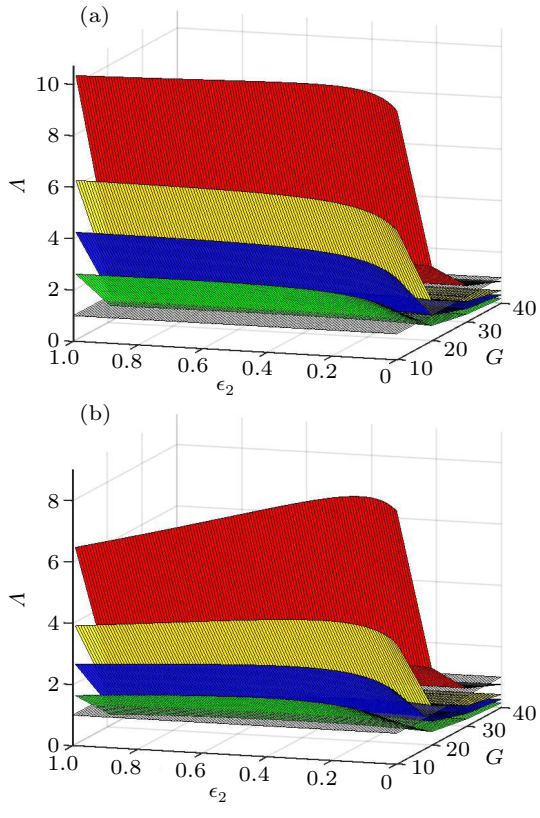


Fig. 13. Multi-structured entangled state versus classical state. Meanings of panels (a) and (b), as well as the colored surfaces, are the same as those in Fig. 12.

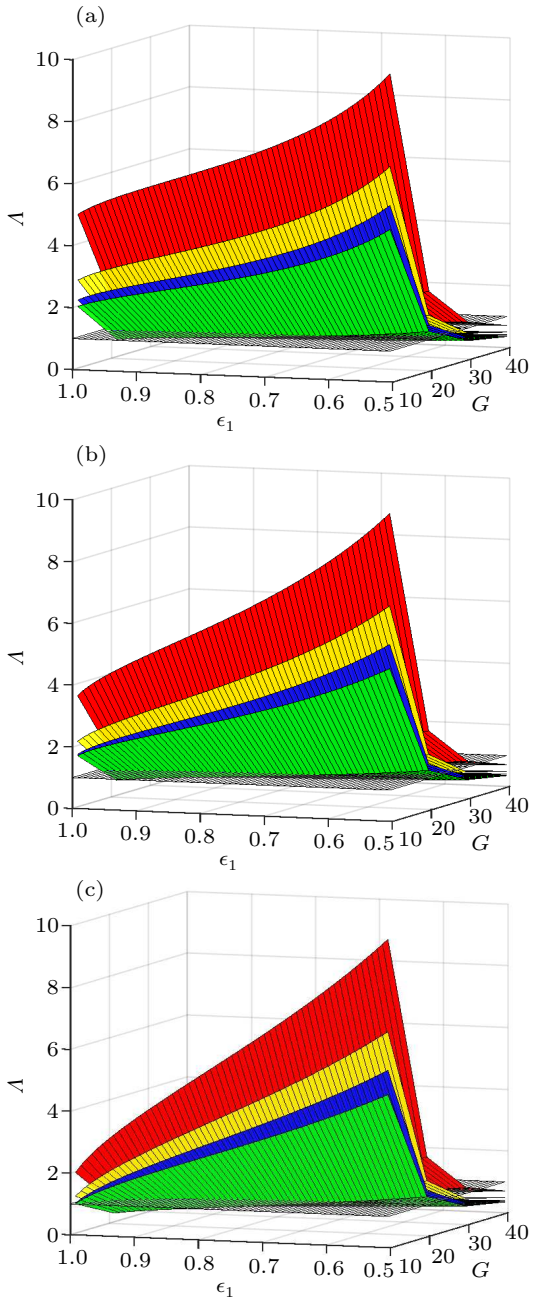


Fig. 14. Multi-structured entangled state versus classical state. Panel (a) represents the simulation results for $\varepsilon_2 \approx 0.3$; panel (b) represents the simulation results for $\varepsilon_2 \approx 0.6$; panel (c) represents the simulation results for $\varepsilon_2 \approx 0.9$ Meaning of the various colored surfaces or planes in the figure is identical to that in Fig. 12.

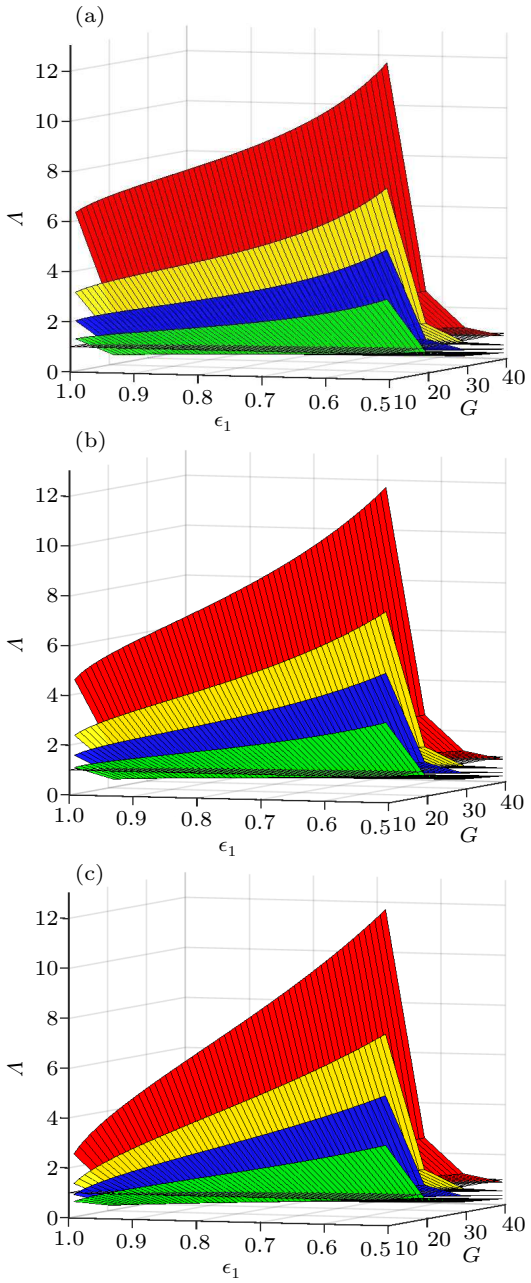


Fig. 15. Multi-structured entangled state versus partially entangled state. Meanings of panels (a)–(c), as well as the colored surfaces, are identical to those in Fig. 14.

The simulation results in Fig. 13 are essentially identical to those in Fig. 12. As ε_2 increases, the gain initially increases and then decreases, reaching its maximum when ε_2 is relatively small. The smaller ε_1 is, the higher the gain. The high value of the gain is due to the fact that the use of a partially entangled state leads to lower time-of-arrival accuracy in a lossy channel.

Overall, as the degree of entanglement among these groups ε_1 decreases, the transmission efficiency η also diminishes, making it more suitable to adopt a multi-structured entangled state to measure the accuracy of the mean TOA.

When ε_2 is fixed at different values, the simulations investigate the relationship between $\Lambda_{gk\text{-cl}}$ and both ε_1 and G for Eq. (51).

Upon examining Figs. 14(a)–14(c), it is evident that the maximal gains are achieved at the same position, and the values of the maximum differ only marginally. First, it is important to note that this point corresponds to the optimal position identified earlier in the lossless channel analysis, where ε_1 is minimized and K is maximized, thereby yielding the maximum values at this specific position. Second, the slight difference among the maximal gains for the surfaces in the same color is still due to the interplay between the transmission efficiency η and the ratio of bandwidth ξ_0 discussed before. For

instance, in Fig. 12(a), the red surface at $G = 10$ demonstrates that the precision gain does not significantly change with variations in ε_2. Therefore, in Fig. 14, the values of the maximum gains show little difference.

As ε_1 increases, ξ_0 decreases, resulting in the impact of varying values of ε_2 on gains becoming significantly more pronounced. When ε_2 is a small value, the gain diminishes slowly, as the precision within each group is ensured. Compared with Fig. 9, it is observed that when the number of groups G is small, the simulation results closely resemble those under a lossless channel. This highlights the advantages of employing a multi-structured entangled state, where, with a larger number per group K, the received groups can be sufficiently ensured.

When ε_2 is fixed at different values, the simulations investigate the relationship between $\Lambda_{gk\text{-part}}$ and both ε_2 and G for Eq. (52).

The simulation results of Fig. 15 are essentially the same as those of Fig. 14. As ε_1 increases, the gain decreases; the smaller ε_2 is, the slower the gain diminishes.

Overall, the greater degree of entanglement of ε_2 and the lower transmission efficiency η, make it more suitable to adopt a multi-structured entangled state.

4. Conclusion

In this paper, we employ partially entangled states within the pulsed quantum ranging scheme, with the goal of alleviating the effects of the photon loss on measurement precision. First, the paper explains why the use of a partially entangled state can effectively reduce the impact of photon loss by introducing the concept of entanglement degree. Under a lossless channel, the higher the degree of entanglement, the greater the precision achieved, a consequence of the precision enhancement induced by entanglement. However, under a lossy channel, the coherence inherent in the partially entangled state continues to allow us to extract the arrival time information of the received photons, even in the face of photon loss. We further configure the partially entangled states into the multi-structured entangled state, which can utilize all the received photon information in the event of photon loss. In addition, the correlations between the quantum states within the multi-structured entangled state have been elucidated. Simulations reveal that by employing the multi-structured entangled state, higher precision can be achieved under identical conditions by adjusting the parameters ξ_0 and K.

Acknowledgments

Project supported by the National Natural Science Foundation of China (Grant No. 62071363) and the Key Research and Development Projects of Shaanxi Province, China (Grant No. 2021LLRH-06).

References

[1] Boto A N, Kok P, Abrams D S, Braunstein S L, Williams C P and Dowling J P 2000 *Phys. Rev. Lett.* **85** 2733
[2] Walls D F 1983 *Nature* **306** 141
[3] Giovannetti V, Lloyd S and Maccone L 2001 *Nature* **412** 417
[4] Giovannetti V, Lloyd S and Maccone L 2004 *Science* **306** 1330
[5] Giovannetti V, Lloyd S and Maccone L 2011 *Nat. Photonics* **5** 222
[6] Goda K, Miyakawa O, Mikhailov E E, Saraf S, Adhikari R, McKenzie K, Ward R, Vass S, Weinstein A J and Mavalvala N 2008 *Nat. Phys.* **4** 472
[7] Schnabel R, Mavalvala N, McClelland D E and Lam P K 2010 *Nat. Commun.* **1** 121
[8] D'Ariano G M, Lo Presti P and Paris M G A 2001 *Phys. Rev. Lett.* **87** 270404
[9] Fabre C, Fouet J B and Maître A 2000 *Opt. Lett.* **25** 76
[10] Pittman T B, Shih Y H, Strekalov D V and Sergienko A V 1995 *Phys. Rev. A* **52** R3429
[11] Cimini V, Gianani I, Ruggiero L, Gasperi T, Sbroscia M, Roccia E, Tofani D, Bruni F, Ricci M A and Barbieri M 2019 *Phys. Rev. A* **99** 053817
[12] Nasr M B, Goode D P, Nguyen N, Rong G, Yang L, Reinhard B M, Saleh B E A and Teich M C 2009 *Opt. Commun.* **282** 1154
[13] Taylor M A and Bowen W P 2016 *Phys. Rep.* **615** 1
[14] Bahder T B and Golding W M 2003 *AIP Conf. Proc.* **734** 395
[15] Zhuang Q 2021 *Phys. Rev. Lett.* **126** 240501
[16] Gao L, Zheng L, Lu B, Shi S, Tian L and Zheng Y 2024 *Opt. Lett.* **13** 294
[17] Sun X, Li W, Tian Y, Li F, Tian L, Wang Y and Zheng Y 2022 *Phys. Rev.* **10** 2886
[18] Li W, Ju M, Li Q, Li R, Yao W, Wu Y, Wang Y, Tian L, Shi S and Zheng Y 2024 *Chin. Opt. Lett.* **22** 072701
[19] Kang G, Feng J, Cheng L, Li Y and Zhang K 2023 *Chin. Phys. B* **32** 104204
[20] Giovannetti V, Lloyd S and Maccone L 2002 *Phys. Rev. A* **65** 022309
[21] Shapiro J H 2003 *Proc. SPIE* **5113** 31
[22] Lloyd S 2008 *Science* **321** 1463
[23] Tan S-H, Erkmen B I, Giovannetti V, Guha S, Lloyd S, Maccone L, Pirandola S and Shapiro J H 2008 *Phys. Rev. Lett.* **101** 253601
[24] Gao W L, Xu L P and Zhang H 2023 *Opt. Express* **31** 41887
[25] Burnham D C and Weinberg D L 1970 *Phys. Rev. Lett.* **25** 84
[26] Chen J, Li X and Kumar P 2004 *Proc. SPIE* **5551** 121
[27] Law C K and Eberly J H 2004 *Phys. Rev. Lett.* **92** 127903
[28] Fedorov M, Efremov M, Kazakov A, Chan K, Law C and Eberly J 2004 *Phys. Rev. A* **69** 052117
[29] Yang C Y, Wu D W, Yu Y L and Zhang H 2011 *J. Beijing Univ. Posts Telecommun.* **34** 33 (in Chinese)